Journal of The Electrochemical Society, **149** (5) A586-A590 (2002)
0013-4651/2002/149(5)/A586/5/$7.00 © The Electrochemical Society, Inc.

Study of $LiBF_4$ as an Electrolyte Salt for a Li-Ion Battery

S. S. Zhang,*,z K. Xu, and T. R. Jow***

U.S. Army Research Laboratory, Adelphi, Maryland 20783, USA

Using 3:7 (wt) ethylene carbonate/ethylmethyl carbonate mixed solvent, we comparatively studied $LiBF_4$ and $LiPF_6$ as solutes for the electrolyte of a Li-ion battery. Results showed that the $LiBF_4$-based electrolyte passivates Al (used as a current collector of the cathode) better than the $LiPF_6$-based one does, while the latter has higher ionic conductivity. It was found that the graphite electrode and the lithium nickel-based mixed oxide cathode have similar lithiation and delithiation cycling behaviors in these two electrolytes. While the difference in the cycling performance of the Li-ion cells using either the $LiBF_4$ or $LiPF_6$-based electrolyte at ambient temperature is negligible. Compared with the one using $LiPF_6$-based electrolyte, the Li-ion cell using $LiBF_4$-based electrolyte is less moisture sensitive and shows much better cycling performance at elevated temperatures. Such a cell could perform even if the electrolyte contained up to 620 ppm of water. The cell also could perform at 60°C with the electrolyte containing 80 ppm of water. At higher temperatures such as 80°C, the Li-ion cell suffered from a severe capacity fading, which is believed to be associated with the irreversible reactions between electrolyte and electrodes.
 [DOI: 10.1149/1.1466857]

Manuscript submitted July 23, 2001; revised manuscript received November 8, 2001. Available electronically March 29, 2002.

Li-ion batteries have been widely used in portable electronic devices such as cellular phones, camcorders, and laptop computers, because of their relatively high specific energy density and power density.[1] In the state-of-the-art Li-ion batteries, most manufacturers use Al foil as cathode current collector and $LiPF_6$ as electrolyte salt. Al is selected as a current collector material mainly because it can naturally form an oxide-based surface layer and withstand high potentials at which the cathode operates. Unfortunately, such a stabilization of the Al only exists in the electrolytes composed of a limited number of lithium salts.[2] The salts that passivate and protect Al well can be used as a solute of the electrolytes. Among commercially available lithium salts, $LiPF_6$ and $LiBF_4$ are known to be capable of providing the electrolyte solutions that are less corrosive to the Al material. Recently, $LiPF_6$ has been a dominant solute for the electrolyte of Li-ion batteries due to these advantages: (*i*) forming a stable solid electrolyte interface (SEI) film on the graphite electrode,[3] (*ii*) providing high ionic conductivity (~10 mS/cm at room temperature) in the nonaqueous electrolytes,[4,5] and (*iii*) being a fire retardant.[6] The most obvious drawbacks of $LiPF_6$ are its thermal instability[7] and moisture sensitivity.[8] It has been reported[7] that $LiPF_6$ thermally decomposes into PF_5 and LiF even at 85°C in the presence of electrolytes. The resulting PF_5 can react with electrolyte solvents, to form gaseous products and move the thermal decomposition of $LiPF_6$ forward. On the other hand, in the presence of moisture, the $LiPF_6$ readily hydrolyzes into toxic POF_3 and HF, which has been identified to be a key source for dissolution of the cathode active materials, especially spinel $Li_xMn_2O_4$.[9] Therefore, Li-ion batteries using $LiPF_6$ salt can operate well only in low moisture electrolyte and near room temperature (−20 to 60°C).[10] To expand the working ambient of Li-ion batteries, it is desirable to replace $LiPF_6$ with more stable lithium salt in the electrolyte of Li-ion batteries.

As early as the mid-1980s, $LiBF_4$ was studied as a solute for the electrolyte of secondary lithium batteries.[11] However, it has not been used in the Li-ion battery, because the electrolytes made of $LiBF_4$ have a relatively low ionic conductivity. More important, this may be due to its inability to form a stable SEI film on the graphite electrode. We believe that relatively low conductivity of the $LiBF_4$-based electrolyte would be made up by its good thermal stability and less moisture sensitivity if the SEI problem could be resolved.

In this work, we comparatively study electrochemical behaviors of the graphite anode and lithium nickel-based mixed oxide cathode in the electrolytes prepared by dissolving 1 mol either $LiPF_6$ or $LiBF_4$ into a 3:7 (wt) EC/EMC mixed solvent. We report on electrochemical corrosion of the Al material and ionic conductivity of the electrolytes. Cycling performance of the Li/graphite, Li/cathode, and graphite/cathode button cells employing $LiBF_4$-based electrolyte is also discussed.

Experimental

Solvents ethylene carbonate (EC, 99.95%, Grant Chemical) and ethylmethy carbonate (EMC, 99.9%, EM Industries, Inc.), and salts, $LiPF_6$ and $LiBF_4$ (both from Stella Chemifa Corporation), were used as received. Electrolyte with a composition of either 1 mol $LiPF_6$ or 1 mol $LiBF_4$, 3:7 EC/EMC (wt) was prepared in an argon-filled glove box with both water and oxygen content of less than 20 ppm. Water content of the electrolytes was determined by Karl-Fischer titration using a Mettler DL 37 KF coulometer. Graphite electrode and cathode films provided by SAFT America were used. Active material of the cathode was a lithium nickel-based mixed oxide, hereinafter abbreviated as cathode for the purpose of convenient description. Specific capacity of the anode-cathode couple is 0.93 mAh/cm^2, which was typically obtained between 2.5 and 3.9 V in a Li-ion cell.

An EG&G PAR potentiostat/galvanostat model 273A controlled by a personal computer was used for the measurements of linear sweep voltammetry and cyclic voltammetry. Passivation current of the Al was recorded in a three-electrode cell by linear potential sweeping at 1.0 mV/s. An Al wire (99.999%, diam = 1.0 mm, Aldrich), which had a 10 mm length exposed to the electrolyte by wrapping it with a thermally shrinkable Teflon tube, was used as a working electrode, and lithium foils were used as a counter and reference electrodes. A combination of Solartron SI 1287 electrochemical interface and SI 1260 impedance/gain-phase analyzer, which was driven by CorrWare and Zplot software, was used to measure impedance spectrum of the cells. Ionic conductivity of the electrolytes was determined by measuring impedance of the electrolytes in a two-platinum-electrode cell having a cell constant of 1.586 cm^{-1}. Using Rayovac's BR2335 button cell cans, Li-ion cells (graphite/cathode) and Li half-cells (Li/cathode and Li/graphite, respectively) were assembled in the same glove box. The electrode area in Li-ion cells was 1.27 cm^2 for graphite anode and 0.97 cm^2 for cathode, respectively, while those in half-cells were all 1.27 cm^2. Amount of the electrolyte in all above button cells was 0.15 mL.

A cyclic voltammogram (CV) of the graphite electrode and the cathode was recorded at a scanning rate of 0.01 mV/s. Cycling test of the button cells was performed on a Maccor series 4000 tester at a constant current density of 0.5 mA/cm^2. For a Li/graphite cell,

* Electrochemical Society Active Member.
** Electrochemical Society Student Member.
z E-mail: szhang@mail.com

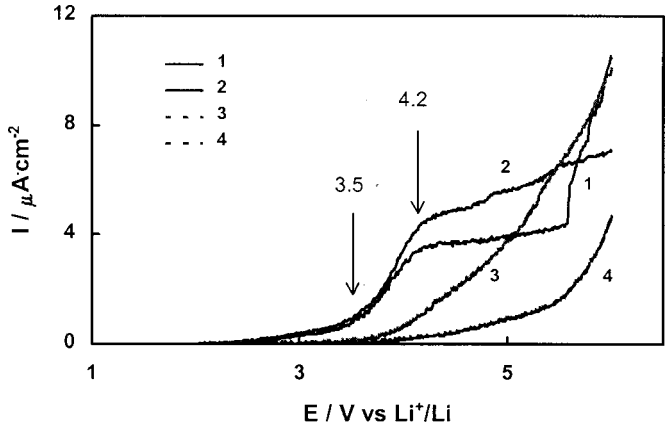

Figure 1. Response of passivation current of Al electrode to the potential in the electrolytes prepared by dissolving 1 mol lithium salt into 3:7 EC/EMC mixed solvent, which was recorded at a sweeping rate of 1.0 mV/s. (1) 1st sweep in $LiPF_6$, (2) 1st sweep in $LiBF_4$, (3) 2nd sweep in $LiPF_6$, and (4) 2nd sweep in $LiBF_4$.

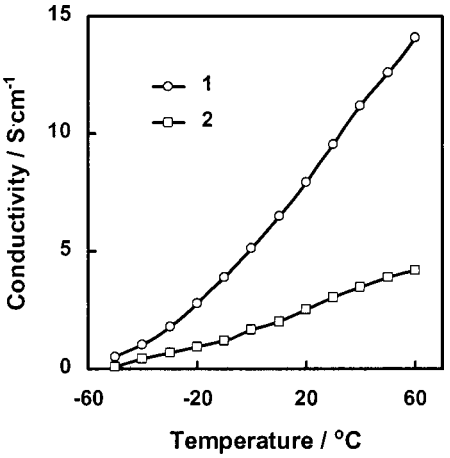

Figure 2. Ionic conductivity of the electrolytes as a function of the temperature. (1) 1 mol $LiPF_6$ 3:7 EC/EMC and (2) 1 mol $LiBF_4$ 3:7 EC/EMC.

current density was 0.5 mA/cm^2 and cutoff voltage was 0.002/1.0 V. Li-ion cells were cycled at 0.5 mA/cm^2 between 2.5 and 3.9 V with a taper of 20 min at 3.9 V after the charging voltage reached 3.9 V. A Tenney environmental oven series 942 was used to provide an elevated temperature condition for the test. AC impedance of the button cell was potentiostatically measured by applying a dc potential bias of 3.9 V and an ac oscillation of 5 mV over the frequency range 100 kHz to 0.01 Hz after the cell had been charged to 3.9 V at 0.5 mA/cm^{2}and remained at 3.9 V for 20 min. The obtained impedance spectra were analyzed by using ZView software (Scribner and Associates, Inc.).

Results and Discussion

Al stability in electrolyte.—Stability of Al material in the electrolyte would be the first consideration for the evaluation of a lithium salt, since the state-of-the-art Li-ion batteries mostly use Al foil as a current collector for the cathode. In this work, we simply used linear sweep voltammetry (LSV) to examine the qualification of $LiBF_4$ as a salt in an electrolyte of Li-ion battery. Figure 1 shows response of the passivation current of Al to the applied potential in the electrolytes composed of 3:7 (wt) EC/EMC mixed solvent and $LiPF_6$ or $LiBF_4$, respectively. Over the potential range of 2-6 V, passivation current of the Al is below 12 μA/cm^2 in both electrolytes with a little difference in the current-potential (I-E) response. A small anodic current begins to appear at 2.8 V *vs.* Li^+/Li and shows a rapid increase at around 3.5 V (curves 1 and 2). However, the increase of the anodic current obviously gets slow as the potential is higher than 4.2 V, forming an S-shaped I-E response. This is a typical characteristic of the electrochemical passivation of the Al in the electrolytes. Note that passivation current of the Al increases abruptly at 5.6 V in $LiPF_6$-based electrolyte, which may originate from a partial breakdown of the passivation film. This condition means that passivation film of Al formed with $LiPF_6$ is not as stable as that formed with $LiBF_4$. More important, the passivation current of the Al electrode becomes much lower in the subsequent sweep in both $LiPF_6$ and $LiBF_4$-based electrolytes (curves 3 and 4), showing that a protective passivation film has been formed on the surface of Al in both cases. Results described above reveal that $LiPF_6$ and $LiBF_4$ are suitable for use in a Li-ion battery. It has been proven[12] that, in $LiPF_6$-based electrolyte, the Li and P are the predominant adsorbed species on the surface layer of Al foil. Therefore, we believe that the phosphor from $LiPF_6$ and the boron from $LiBF_4$ other than the fluoride are likely participants in the formation of the passivation film on the Al surface. To verify this, we examined (in a separate experiment) the effect of fluoride on the corrosion of Al material in a CF_3SO_3Li-based electrolyte by intentionally dissolving a small amount (2%) of $C_4F_9SO_2F$ in the electrolyte. Consequently, Al still is severely corroded by CF_3SO_3Li without visible improvement, although $C_4F_9SO_2F$ can be partially dissociated into free F^- anions.

Ionic conductivity.—Figure 2 compares ionic conductivity of two electrolytes prepared by dissolving either 1 mol $LiPF_6$ or 1 mol $LiBF_4$ in 3:7 (wt) EC/EMC mixed solvent. It is shown that, over the measured temperature range (−50 to 60°C), the $LiPF_6$-based electrolyte provides higher ionic conductivity, especially at elevated temperatures. This may be ascribed to the larger radius of the PF_6^- anion, which favors delocalization of the negative charge and promotes dissociation of the salt in the solvent. Normally, ionic conductivity of the EC-based electrolytes sharply decreases at a certain temperature below −10°C, because of the crystallization of EC solvent. However, we did not observe this sharp decline in the ionic conductivity even at −50°C, which is due to supercooling in the absence of nucleating particles.[13] It is known that poor performance of Li-ion batteries at elevated temperatures (>50°C) and low temperatures (<−20°C) is a major concern with their applications, especially in hybrid electric vehicles (HEVs) and electric vehicles (EVs). In view of the electrolyte salt, $LiPF_6$ is thermally instable and its decomposition products (PF_5) can initiate productive reactions with electrolyte solvents.[7] This drawback of $LiPF_6$ salt has been one of the main limitations to the high temperature performance of Li-ion batteries. On the other hand, it has been identified[14,15] that the limitation to the low temperature performance of Li-ion batteries is caused by either low ionic conductivity of SEI film on graphite surface or low diffusivity of Li^+ ions within graphite instead of ionic conductivity of the electrolyte between two electrodes. Therefore, the relative low ionic conductivity of the $LiBF_4$-based electrolyte could be accepted in Li-ion battery if the thermally stable $LiBF_4$ can replace $LiPF_6$ without reducing the formation of a protective SEI film on graphite surface. With above background in mind, we focus our effort on evaluating the cycling behavior of the graphite electrode and cathode in $LiBF_4$-based electrolyte.

Cycling performance of graphite electrode and cathode.—Figure 3 shows CVs of the graphite electrode in $LiPF_6$ and $LiBF_4$-based electrolytes, respectively, which were recorded during the first cycle at a slow scanning rate of 0.01 mV/s. During intercalation of Li ions into graphite electrode, there appeared three overlapped reductive current peaks in the CV between 0.3 and 0 V *vs.* Li^+/Li, which reflects multiple-stage intercalation of Li ions into graphite. The inset of Fig. 3 plots the CV of the third cycle, which was obtained from the $LiBF_4$-based electrolyte at a very slow scanning rate of

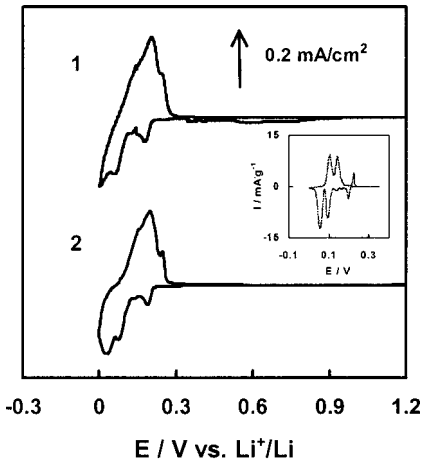

Figure 3. CV of the graphite electrode in different electrolytes, which was recorded during the first cycle at a scanning rate of 0.01 mV/s. (1) 1 mol $LiPF_6$ 3:7 EC/EMC and (2) 1 mol $LiBF_4$ 3:7 EC/EMC.

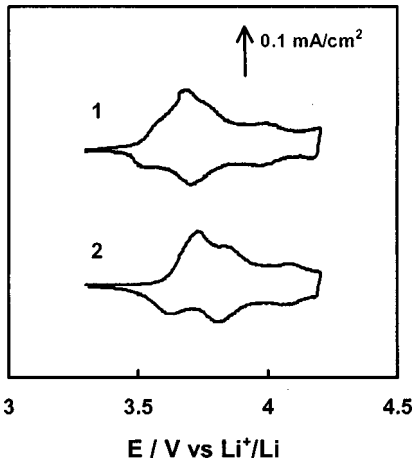

Figure 5. CV of the cathode in different electrolytes, which was recorded during the first cycle at a scanning rate of 0.01 mV/s. (1) 1 mol $LiPF_6$ 3:7 EC/EMC and (2) 1 mol $LiBF_4$ 3:7 EC/EMC.

0.001 mV/s. The inset indicates that these three reversible transitions occur at 19.6/22.6, 9.1/14.3, and 5.3/10.6 mV, respectively. According to the amount of involved charges, Levi *et al.*[16] assigned these peaks to the following major phase transitions: $LiC_{72} + Li \rightleftarrows 2LiC_{36}$, $4LiC_{27} + 5Li \rightleftarrows 9LiC_{12}$, and $LiC_{12} + Li \rightleftarrows 2LiC_6$. It is calculated from Fig. 3 that, during the first cycle, coulombic efficiency (CE) of the graphite electrode is 82% with $LiPF_6$-based electrolyte and 89% with $LiBF_4$-based one, respectively. A difference is that the $LiPF_6$-based electrolyte produces a bit larger irreversibly reductive current at the voltages of above 0.3 V, which leads to a relatively low CE. The voltage-capacity curve of the first cycle for the Li/graphite cells obtained at a constant current density of 0.5 mA/cm^2 in different electrolytes is illustrated in Fig. 4, in which the inset is a part selected from the voltage range of below 0.3 V. Again, it is indicated that the intercalation process of Li ions into the graphite electrode consists of three major stages, consistent with the CV results discussed above. However, the CE results estimated from Fig. 4 are opposite to those calculated from CV measurement (see Fig. 3). The CE of the graphite electrode was 90% in $LiPF_6$-based electrolyte *vs.* 82% in the $LiBF_4$-based one. The inset of Fig. 4 shows that, in comparison to $LiPF_6$, $LiBF_4$ salt leads to slightly higher potentials for the lithiation and delithiation cycle of graphite electrode, which will reduce the overall voltage of Li-ion batteries and cause a small decrease of the battery power.

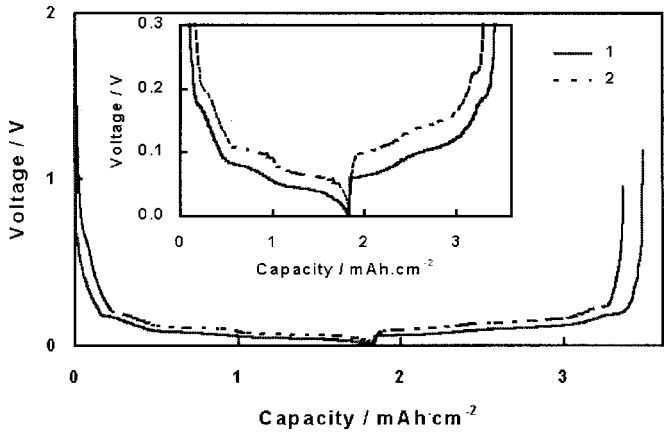

Figure 4. Voltage change of the Li/graphite cell with capacity in different electrolytes, which was recorded during the first cycle at a cycling rate of 0.5 mA/cm^2 between OCV and 0.002 V. Inset is a part selected from the voltage range of between 0.3 and 0.002 V. (1) 1 mol $LiPF_6$ 3:7 EC/EMC and (2) 1 mol $LiBF_4$ 3:7 EC/EMC.

Figure 5 compares cyclic voltammograms of the cathode in $LiPF_6$ and $LiBF_4$-based electrolytes, which were recorded during the first cycle at 0.01 mV/s. The CV of the cathode consists of three pairs of wide and overlapped current peaks, Typically, these three pairs of current peaks of the cathode in $LiBF_4$-based electrolyte are located at 3.75/3.60, 3.87/3.79, and 4.11/4.07 V, respectively. Lee *et al.* reported[17] that, during delithiation and lithiation cycle, the pure $LiNiO_2$ cathode undergoes three phase continuous transitions, *i.e.*, hexagonal (H_1) $\rightleftarrows$ monoclinic (M) $\rightleftarrows$ hexagonal (H_2) $\rightleftarrows$ hexagonal (H_3). With doping by the second metal such as cobalt, the multiphase structure of $LiNiO_2$ is gradually diminished and finally transfers to single phase. It is determined from Fig. 5 that the CE of the cathode is 86.3% with $LiPF_6$ and 96.5% with $LiBF_4$. High CE of 96.5% as obtained from the $LiBF_4$-based electrolyte indicates that $LiBF_4$ salt may help to reduce the reaction of cathode and electrolyte solvents, which is speculated to form a surface layer on the cathode surface. Several phenomena have been used as explanations of the initial irreversible capacity of the $LiNiO_2$-based cathodes. One phenomenon, reported by Delmas *et al.*[18] is the structural change of $LiNiO_2$-based materials due to collapsing of Ni^{2+} ions in the Ni^{3+} layers into the delithiated lithium layers. A second one, given by Aria *et al.*,[19] is the formation of electrically isolated regions in the cathode particles as the x value in Li_xNiO_2 is reduced beyond 0.8. A third one presented by Matsuo *et al.*[20] is the formation of a surface layer on the cathode surface due to the reaction between cathode and electrolyte solvents.

Although the third phenomenon was observed directly from the spinel $LiMn_2O_4$ cathode,[20] we recently observed a similar condition in the $LiNiO_2$-based cathode.[21] It is obvious that, in the present case, the observed difference in the initial CE between $LiPF_6$ and $LiBF_4$-based electrolytes raises from the salt instead of the cathode material and electrolyte solvents.

Cycling performance of graphite/cathode cell.—Figure 6 displays discharge capacities of the graphite/cathode cell employing either $LiPF_6$ or $LiBF_4$-based electrolyte as a function of cycle number, which were obtained by cycling the cell between 2.5 and 3.9 V at room temperature. Water content of these two electrolytes is less than 25 ppm, determined by Karl Fischer titration. It is seen from Fig. 6 that, during the initial ~100 cycles, discharge capacities of the cells are independent of the salts used in the electrolyte, and that both cells deliver a similar discharge capacity of 0.96-0.99 mAh/cm^2. As the cycle number further extends, capacity

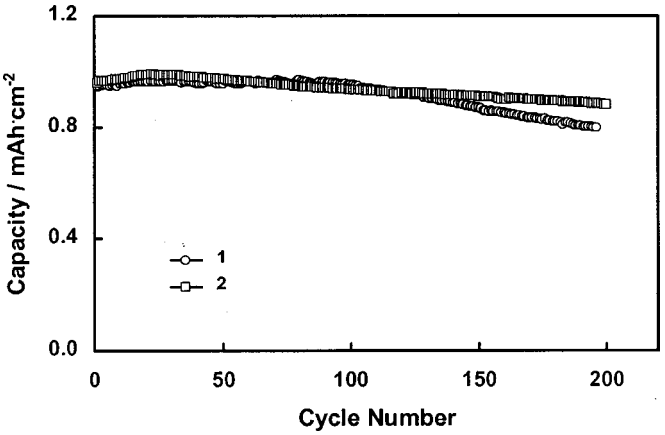

Figure 6. Discharge capacities of the graphite/cathode cells using different electrolytes at room temperature, which were measured at a constant current density of 0.5 mA/cm^2 between 2.5 and 3.9 V with a taper of 20 min after charging voltage reached 3.9 V. (1) 1 mol $LiPF_6$ 3:7 EC/EMC and (2) 1 mol $LiBF_4$ 3:7 EC/EMC.

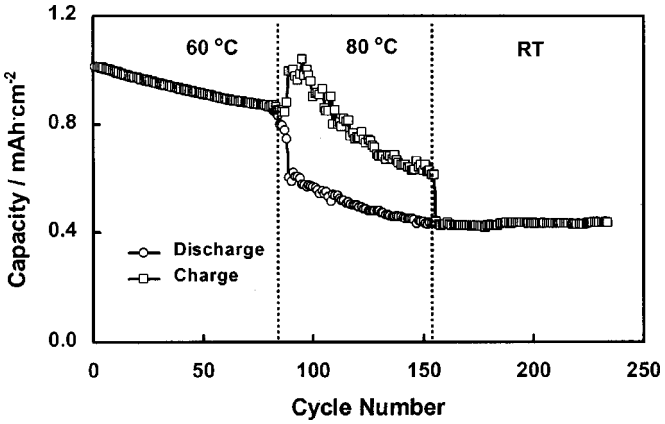

Figure 8. Charge and discharge capacities of the graphite/cathode cell *vs.* the cycle number at various temperatures. The electrolyte was a 1 mol $LiBF_4$ 3:7 EC/EMC solution with 80 ppm of water. Current density was 0.5 mA/cm^2 and cutoff voltage was 2.5 V/3.9 V with a taper of 20 min after charging voltage reached 3.9 V.

fading of the cell using $LiPF_6$ accelerates, while that using $LiBF_4$ still remains at a slow rate. Because water content of these electrolytes is low (<25 ppm), we believe that the difference in the observed capacity fading rate is due to the poor thermal stability of $LiPF_6$ salt. Upon over 100 cycles, $LiPF_6$ may slowly decompose to form highly reactive PF_5, which subsequently reacts with electrolyte solvents and further causes an increase in internal impedance of the cell. As a result of $LiPF_6$ thermal decomposition, capacity fading of the cell is significantly accelerated.

Figure 7 compares the effect of water content on the cycling performance of graphite/cathode cells in different $LiBF_4$-based electrolytes. It is observed that, at room temperature, water content even as high as 620 ppm negligibly affects cycling performance of the cells. This good feature is ascribed to the relatively lower moisture sensitivity of the $LiBF_4$ salt. As the temperature rises to 50°C, the cell employing $LiPF_6$-based electrolyte fails shortly (not shown in the figure), and the effect of water content on the cycling performance becomes noticeable. When the water content in the $LiBF_4$-based electrolyte is less than 80 ppm, the cell still can perform at 50°C with a very low capacity fading rate (curves 1 and 2 of Fig. 7). However, the cell containing 620 ppm of water in the electrolyte suffers fast capacity fading at 50°C (curve 3 of Fig. 7). This is not surprising; under such a condition, water will react readily with lithiated graphite (Li_xC_6) at the anode, while being oxidized at the cathode.

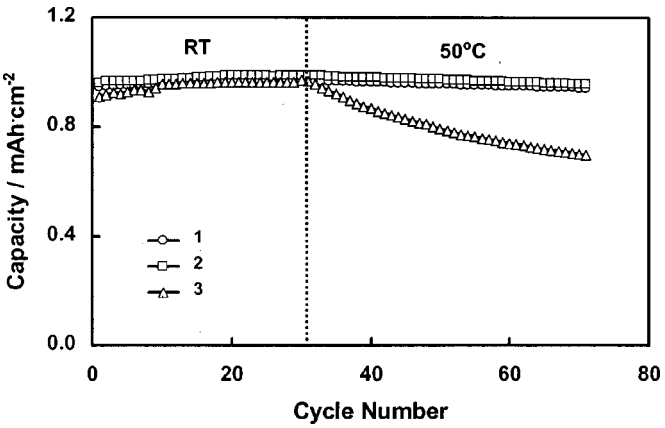

Figure 7. Discharge capacities of the graphite/cathode cells using 1 mol $LiBF_4$ 3:7 EC/EMC electrolytes with various water content, which were measured at a constant current density of 0.5 mA/cm^2 between 2.5 and 3.9 V with a taper of 20 min after charging voltage reached 3.9 V. (1) 22 ppm, (2) 80 ppm, and (3) 620 ppm.

To find the high temperature limit for the operation of a graphite/cathode cell using $LiBF_4$-based electrolyte, we examined the effect of temperature on the cycling performance. Charge and discharge capacities of the graphite/cathode cell at various temperatures are plotted in Fig. 8 as a function of the cycle number, which were obtained after the cell had cycled 200 times at room temperature. At 60°C, the CE of charge and discharge cycle remains constant at more than 98%, in spite of an accelerated capacity fading as compared to that observed at room temperature. It is estimated that the cell lost 17% of the capacity after 80 cycles at 60°C, which is indicated by an increase in internal impedance of the cell (discussed later). As the temperature was further increased to 80°C, discharge capacity of the cell abruptly fell from 0.87 to 0.62 mAh/cm^2 while the charge capacity jumped from 0.87 to 1.0 mAh/cm^2. After this, both charge and discharge capacities of the cell fade rapidly. It is shown in Fig. 8 that, while cycling at 80°C, the cell discharges much lower capacity than that charged and presents a very low CE. This observation reveals that cycling the cell at 80°C produces a large amount of irreversible capacity.

We believe that this irreversible capacity is associated with electrolyte decomposition and is the origin for permanent capacity loss. Importantly, discharge capacity of the cell cannot be recovered when the temperature is lowered back to room temperature, at which the CE of the cell returns near unity, as displayed between cycles 157 and 237 in Fig. 8. In other words, the capacity loss during cycling at 80°C is permanent.

Impedance of graphite/cathode cell.—To understand the reason for capacity loss, we studied impedance of the cell employing 1 mol $LiBF_4$ 3:7 EC/EMC electrolyte. Figure 9 plots impedance spectra of the graphite/cathode cell, which were recorded at charged state (3.9 V) after the cell had performed for a certain number of cycles at various temperatures. Typically, the impedance spectra are composed of two flattened and overlapped semicircles at high and medium frequency regions as well as a sloping straight line at low frequency regions. Such spectra can be analyzed with an equivalent circuit as shown in Fig. 10, where R_e is the resistance of electrolyte and electrodes, C_{SEI}/R_{SEI} is the capacitance/resistance of SEI layer on the electrodes, and C_{ad}/R_{ad} is the capacitance/resistance of adsorbed layer that is located in outer layer of the SEI film.[22] We link the semicircle at medium frequencies to adsorbed layer instead of

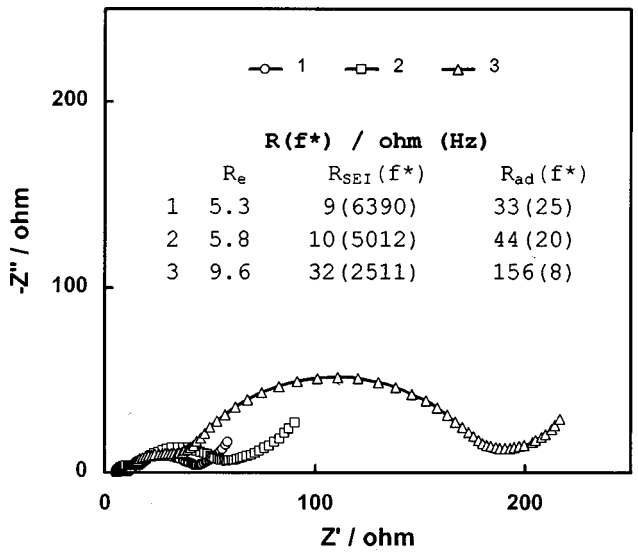

Figure 9. Impedance spectra of the graphite/cathode cell after various cycle numbers, which were recorded at 3.9 V over the frequency range from 10^5 to 0.01 Hz. The electrolyte was a 1 mol $LiBF_4$ 3:7 EC/EMC solution with 80 ppm of water. Current density was 0.5 mA/cm^2 and cutoff voltage was 2.5 V/3.9 V with a taper of 20 min after charging voltage reached 3.9 V. (1) after 200 cycles at room temperature, (2) after 80 cycles at 60°C following spectrum 1, and (3) after 76 cycles at 80°C following spectrum 2.

the charge-transfer process of Li^+ ions on the basis of these considerations: (*i*) the frequency (f^*) at the top of the semicircle is rather high for the charge-transfer process, (*ii*) the resistance of the semicircle varies too much for the charge-transfer process that should be more dependent of the composition of the electrodes, and (*iii*) the large irreversible capacity observed during the cell cycled at 80°C likely is an additional evidence for the presence of adsorbed layer since the irreversible reactions inevitably yield insoluble products that within the cell most probably exist in a form of the adsorbed layer.

According to the equivalent circuit, we fitted impedance spectra by using ZView software and listed the data of resistance (R) and frequency (f^*) in Fig. 9. Comparing the R value of impedance spectra 1 (after 200 cycles at room temperature) and 2 (followed by 80 cycles at 60°C), we find only about 10% increase in the R_e and R_{SEI} and about 33% increase in the R_{ad} after the cell was run 80 cycles at 60°C. This implies that the graphite/cathode cell employing a $LiBF_4$-based electrolyte could perform at 60°C. A significant increase in the R_e and R_{SEI} is observed after the cell was further cycled 76 times at 80°C (spectrum 3), which is believed to be associated with the irreversible reactions taking place at 80°C. It is worthy of note that the impedance spectrum of the cell no longer changes after the temperature is lowered back to room temperature, followed by continuously cycling the cell 80 times (not plotted in the figure). We may get some hints from the change of the R_{ad} and f^*_{ad} with the cycle number at various temperatures. Significant increase in the R_{ad} reveals that, during cycling at 80°C, the adsorbed layer has substantially grown and become very resistive, while the change (decrease) in the f^*_{ad} shows that composition of the adsorbed layer has greatly changed. Taking a large amount of permanent capacity loss at 80°C (Fig. 8) into account, we may conclude that the main constituents of the adsorbed layer are the products of irreversible reactions, and that the graphite/cathode cell employing $LiBF_4$-based electrolyte is still unable to stand or perform at 80°C.

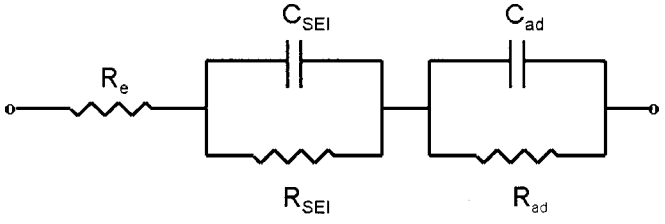

Figure 10. Equivalent circuit used for analysis of the impedance spectra.

Conclusions

$LiBF_4$ and $LiPF_6$ are two commercially available salts capable of passivating and protecting Al in the nonaqueous electrolytes. In the electrolyte composed of either 1 mol $LiBF_4$ or 1 mol $LiPF_6$ salt and a 3:7 (wt) EC/EMC mixed solvent, passivation of the Al material mainly occurs at near 3.5 V *vs.* Li^+/Li. At more positive potentials, passivation current of the Al is lower in $LiBF_4$-based electrolyte than in $LiPF_6$-based one. Compared with the $LiPF_6$-based one, the $LiBF_4$-based electrolyte has lower ionic conductivity, but is able to provide the similar cycling performance for both graphite electrode and lithium nickel-based mixed oxide cathode. As $LiBF_4$ is less moisture-sensitive and more thermally stable, the Li-ion cell employing it performs better at high water content and at elevated temperatures. Such a cell, even with water content as high as 620 ppm, can perform well at room temperature, but its capacity fades significantly at elevated temperatures (50°C). The cell containing 80 ppm of water can perform at 60°C with a coulombic efficiency of more than 98%. At higher temperature (80°C), the cell loses its capacity rapidly because some irreversible reactions takes place, which not only decreases coulombic efficiency of the charge and discharge cycle but also increases internal impedance of the cell.

Acknowledgment

We thank SAFT America, Inc. for providing both graphite electrode and lithium nickel-based mixed oxide cathode films.

U.S. Army Research Laboratory assisted in meeting the publication costs of this article.

References

1. B. A. Johnson and R. E. White, *J. Power Sources*, **70-71**, 48 (1998).
2. (a) W. K. Behl and E. J. Plichta, *J. Power Sources*, **72**, 132 (1998); (b) W. K. Behl and E. J. Plichta, *J. Power Sources*, **88**, 192 (2000).
3. N. Takami, T. Ohsaki, and K. Inada, *J. Electrochem. Soc.*, **139**, 1849 (1992).
4. K. Hayashi, Y. Nemoto, S. I. Tobishima, and J. I. Yamaki, *Electrochim. Acta*, **44**, 2337 (1999).
5. M. S. Ding, K. Xu, S. S. Zhang, K. Amine, G. L. Henriksen, and T. R. Jow, *J. Electrochem. Soc.*, **148**, A1196 (2001).
6. H. Akashi, K. I. Tanaka, and K. Sekai, *J. Electrochem. Soc.*, **145**, 881 (1998).
7. S. E. Sloop, J. K. Pugh, S. Wang, J. B. Kerr, and K. Kinoshita, *Electrochem. Solid-State Lett.*, **4**, A42 (2001).
8. D. Aurbach, M. L. Daroux, P. W. Faguy, and E. Yeager, *J. Electrochem. Soc.*, **134**, 1611 (1987).
9. D. H. Jang, Y. J. Shin, and S. M. Oh, *J. Electrochem. Soc.*, **143**, 2204 (1996).
10. L. J. Krause, W. Lamanna, J. Summerfield, M. Engle, G. Korba, and R. Atanasoski, *J. Power Sources*, **68**, 320 (1997).
11. Y. Matsuda, M. Morita, and T. Yamashita, *J. Electrochem. Soc.*, **131**, 2821 (1984).
12. J. W. Braithwaite, A. Gonzales, G. Nagasubramanian, S. J. Lucero, D. E. Peebles, J. A. Ohlhausen, and W. R. Cieslak, *J. Electrochem. Soc.*, **146**, 448 (1999).
13. S. P. Ding, K. Xu, S. S. Zhang, T. R. Jow, K. Amine, and G. L. Henriksen, *J. Electrochem. Soc.*, **146**, 3974 (1999).
14. H. P. Lin, D. Chua, M. Salomon, H. C. Shiao, M. Hendrickson, E. Plichta, and S. Slane, *Electrochem. Solid-State Lett.*, **4**, A71 (2001).
15. C. K. Huang, J. S. Sakamoto, J. Wolfenstine, and S. Surampudi, *J. Electrochem. Soc.*, **147**, 2893 (2000).
16. M. D. Levi and D. Aurbach, *J. Electroanal. Chem.*, **421**, 79 (1997).
17. K. K. Lee and K. B. Kim, *J. Electrochem. Soc.*, **147**, 1709 (2000).
18. C. Delmas, J. P. Peres, A. Rougier, A. Demourgues, F. Weill, A. Chadwick, M. Broussely, F. Perton, P. Biensan, and P. Willmann, *J. Power Sources*, **68**, 120 (1997).
19. H. Arai, S. Okada, Y. Sakurai, and J. Yamaki, *Solid State Ionics*, **95**, 275 (1997).
20. Y. Matsuo, R. Kostecki, and F. McLarnon, *J. Electrochem. Soc.*, **148**, A687 (2001).
21. S. S. Zhang, K. Xu, and T. R. Jow, Unpublished work.
22. Y. Xia, Y. Zhou, and M. Yoshio, *J. Electrochem. Soc.*, **144**, 2593 (1997).